AIAA JOURNAL
Vol. 42, No. 11, November 2004

Simple Full-Field Method for the Elastic Characterization of Orthotropic Composite Plates

W. O. Wong* and P. Feng†
Hong Kong Polytechnic University, Hong Kong, People's Republic of China
S. R. Reid‡
UMIST, Manchester, England, United Kingdom
and
K. T. Chan§
Hong Kong Polytechnic University, Hong Kong, People's Republic of China

A speckle shearing interferometer with a simple setup is designed and tested for full-field characterization of the elastic properties of isotropic and orthotropic composite plates. The technique is straightforward and provides comparable results obtained by standard methods. The proposed method has the advantages of being noncontact and full field in nature. Beam specimens cut from the plate were loaded under the standard four-point bending configuration. Gradients of bending deformation are measured by the speckle shearing interferometer directly. Curvature of each bended beam is calculated from the slope of the fitted line of the gradient data. The elastic moduli and Poisson's ratios of the plate material are determined from the curvature of the beam specimens. Comparing the present approach to other full-field techniques reported in literature that are mostly based on deformation measurement of a specimen subjected to a complicated load field, the present method is much easier to apply, and the image analysis procedure is much simpler.

I. Introduction

TO design and model structural composite parts correctly, it is necessary to determine accurately the elastic properties of the constitutive materials. Standard tests, always mechanical, are available to characterize composites.[1–3] These tests, which employ many kinds of local strain gauges, require that the state of stress within the tested section be uniform for correct experimental data interpretation. This is not always easy to achieve especially in the case of shear characterization in which parasitic effects caused by the material anisotropy can significantly bias the measurements.[4,5] Contrary to the weakness of the mechanical tests, optical methods are noncontact and full field, and so that it is no longer necessary to assume strictly uniform stress in the tested section. With regard to these methods, the difficulties lie in the data processing, usually termed fringe analysis. Fortunately, owing to the development of computer techniques and the phase-shifting technique, fast and precise fringe analysis can be achieved so that direct identification, or even real-time measurement, becomes feasible. Accordingly optical surface displacement methods leading to the surface strains are now seen as ideal substitutes for mechanical strain measurement methods.

Recently, a direct identification approach based on static testing[6,7] and free-vibration measurements[8] for the identification of bending stiffnesses has been proposed by Grédiac et al. The main feature of this approach is that the identification process does not require any iteration, unlike that in Refs. 9 and 10. Grédiac et al. demonstrated the use of moiré-based methods for the measurement of displacement fields. The displacement fringe patterns were demodulated by a phase-stepping method.[11] The strain fields required for the determination of the in-plane stiffnesses were obtained by numerical differentiation of the measured displacement fields. As stated by Grèdiac et al., the strain fields are therefore less accurate, and it would be better to use other optical techniques that can provide the strain fields directly.[7]

Among commonly used optical methods to evaluate deformation, speckle, holographic, and moirè interferometry, all measure the displacement component only. However, stress analysis is usually interested in strains rather than displacements. Strain is obtained by fitting the displacement data numerically and then by differentiating, a procedure that, as noted before, can lead to large errors. Methods are therefore required that can yield fringe patterns that represent the derivatives of the displacement. This is achieved by electronic speckle shearing interferometry (ESSI).[12]

ESSI determines the derivatives or their approximate values of surface displacements. The principle of the measurement is based on the interference of two mutually displaced speckle patterns of the same object. When two speckle patterns corresponding to two different object states, for example, before and after applying the loads, are compared by image subtraction, the correlation fringes connecting the points of equal displacement gradients are formed. The direction of displacement between the two speckle patterns determines the direction of the partial derivative averaged over the shear displacement.[12]

As shown in Sec. IV.D, real-time correlation fringe patterns can be generated with a computerized image grabbing system for recording and processing the speckle interference fields.[13] It thus overcomes the disadvantages of the conventional photographic recording and reconstruction techniques. The value of displacement gradient at each pixel of the inteferogram can be determined by phase-shifting or phase-stepping techniques.[11,14]

Using the proposed method, out-of-plane displacement gradients of beam specimens under a four-point bending configuration are measured. The bending strains can be determined from the slope of the linear displacement gradient function. Bending stiffness can then be calculated by dividing the applied moment by the bending strain.

Received 8 May 2003; revision received 19 April 2004; accepted for publication 5 June 2004.

*Assistant Professor, Department of Mechanical Engineering.
†Research Assistant, Department of Mechanical Engineering; currently Research Student, Department of Mechanical Engineering, Hong Kong University of Science and Technology, Hong Kong, People's Republic of China.
‡Professor, Department of Mechanical, Aerospace and Manufacturing Engineering.
§Associate Professor, Department of Mechanical Engineering.

II. Formulation of the Problem and Parameters of Identification

As far as a fiber-reinforced composite material is concerned, the macromechanical behavior of its laminas is narrated in many relevant textbooks.[1,15] The generalized Hooke's law relating stresses to strains can be written in contracted notation as

$$\{\sigma_i\} = [C_{ij}]\{\varepsilon_j\}, \qquad i, j = 1, \ldots, 6 \tag{1}$$

where $\{\sigma_i\}$, $[C_{ij}]$, and $\{\varepsilon_j\}$ are the stress vector, the stiffness matrix, and the strain vector, respectively.

If there are two orthogonal planes of material property symmetry for a material, symmetry will exist relative to a third mutually orthogonal plane. Define principal material directions to be parallel to the intersections of the three orthogonal planes of material property symmetry. The stress–strain relations in coordinates aligned with the principal material direction are

$$\begin{Bmatrix} \sigma_1 \\ \sigma_2 \\ \sigma_3 \\ \tau_{23} \\ \tau_{31} \\ \tau_{12} \end{Bmatrix} = \begin{bmatrix} C_{11} & C_{12} & C_{13} & 0 & 0 & 0 \\ C_{12} & C_{22} & C_{23} & 0 & 0 & 0 \\ C_{13} & C_{23} & C_{33} & 0 & 0 & 0 \\ 0 & 0 & 0 & C_{44} & 0 & 0 \\ 0 & 0 & 0 & 0 & C_{55} & 0 \\ 0 & 0 & 0 & 0 & 0 & C_{66} \end{bmatrix} \begin{Bmatrix} \varepsilon_1 \\ \varepsilon_2 \\ \varepsilon_3 \\ \gamma_{23} \\ \gamma_{31} \\ \gamma_{12} \end{Bmatrix} \tag{2}$$

For a thin lamina in the 1-2 plane as shown in Fig. 1 or a woven lamina, a plane-stress state is defined by setting

$$\sigma_3 = 0, \qquad \tau_{23} = 0, \qquad \tau_{31} = 0 \tag{3}$$

If the material is orthotropic, the strain–stress relations in Eq. (2) can be reduced to

$$\begin{Bmatrix} \sigma_1 \\ \sigma_2 \\ \tau_{12} \end{Bmatrix} = \begin{bmatrix} Q_{11} & Q_{12} & 0 \\ Q_{12} & Q_{22} & 0 \\ 0 & 0 & Q_{66} \end{bmatrix} \begin{Bmatrix} \varepsilon_1 \\ \varepsilon_2 \\ \gamma_{12} \end{Bmatrix} \tag{4}$$

where Q_{ij} are the so-called reduced stiffnesses for a plane stress state in the 1-2 plane.

Equation (4) can be written in its inverted form:

$$\begin{Bmatrix} \varepsilon_1 \\ \varepsilon_2 \\ \gamma_{12} \end{Bmatrix} = \begin{bmatrix} S_{11} & S_{12} & 0 \\ S_{12} & S_{22} & 0 \\ 0 & 0 & S_{66} \end{bmatrix} \begin{Bmatrix} \sigma_1 \\ \sigma_2 \\ \tau_{12} \end{Bmatrix} \tag{5}$$

where the S_{ij} are the compliances for a plane-stress state in the 1-2 plane. They can be expressed by the engineering constants as

$$\begin{aligned} S_{11} &= 1/E_1 \\ S_{12} &= -\mu_{12}/E_1 = -\mu_{21}/E_2 \\ S_{22} &= 1/E_2 \\ S_{66} &= 1/G_{12} \end{aligned} \tag{6}$$

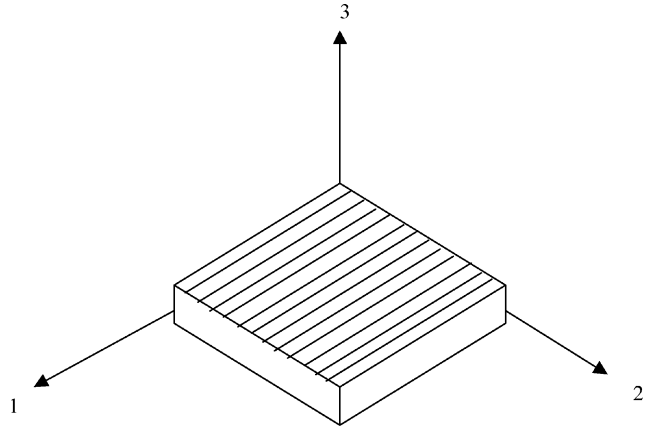

Fig. 1 Geometry of the unidirectional reinforced plate.

The engineering constants are generally the slope of a stress–strain curve (e.g., $E = \sigma/\varepsilon$) or the slope of a strain–strain curve (e.g., $\mu = -\varepsilon_y/\varepsilon_x$ for $\sigma_x = \sigma$ and all other stresses zero). The parameters to be identified are 1) Young's moduli, E_1, E_2; 2) Poisson's ratio, μ_{12}, μ_{21}; and 3) shear modulus G_{12}.

If the x axis chosen is not along the 1 axis but at an angle θ to the 1 axis, the stress–strain relations should be

$$\begin{Bmatrix} \varepsilon_x \\ \varepsilon_y \\ \gamma_{xy} \end{Bmatrix} = \begin{bmatrix} \bar{S}_{11} & \bar{S}_{12} & \bar{S}_{16} \\ S_{12} & \bar{S}_{22} & \bar{S}_{26} \\ \bar{S}_{16} & \bar{S}_{26} & S_{66} \end{bmatrix} \begin{Bmatrix} \sigma_x \\ \sigma_y \\ \tau_{xy} \end{Bmatrix}$$

$$= [T]^T \begin{bmatrix} S_{11} & S_{12} & 0 \\ S_{12} & S_{22} & 0 \\ 0 & 0 & S_{66} \end{bmatrix} [T] \begin{Bmatrix} \sigma_x \\ \sigma_y \\ \tau_{xy} \end{Bmatrix} \tag{7}$$

where

$$[T] = \begin{bmatrix} \cos^2\theta & \sin^2\theta & \sin 2\theta \\ \sin^2\theta & \cos^2\theta & -\sin 2\theta \\ -\sin 2\theta/2 & \sin 2\theta/2 & \cos 2\theta \end{bmatrix}$$

III. Theory of Measurement

The principle of ESSI can be found in the relevant literature (such as Ref. 12), and it is briefly described in the following. The schematic diagram of the optical setup is shown in Fig. 2. The object is a beam specimen as shown in Fig. 3. A charge-coupled-device (CCD) imaging system is used with a shearing lens of the birefringent type. A suitable polarizer is employed to bring the two emerged orthogonally polarized wavefronts to the same polarization to ensure best interference. The frame grabber is controlled by a microcomputer for image processing. A He–Ne laser is used as a light source. Its wavelength is λ. The specimen surface is diffusive to the laser light.

As shown in Fig. 2, the shearing lens brings the rays from two neighboring points P and Q on the object surface to a point O in the CCD camera. The shearing lens is made and aligned to let points P and Q be represented by coordinates (x, y, z) and $(x + \delta x, y + \delta y, z)$, respectively. The shear length is $\sqrt{[(\delta x)^2 + (\delta y)^2]}$, and it should be small enough to obtain sufficient accuracy of gradient measurement along the shear direction $(\delta x, \delta y, 0)$ and good interference of the light beams. The intensity at point O of the image recorded by the camera can be written as[16]

$$I_O = I_P + I_Q + 2\sqrt{I_P I_Q}\cos\,\phi \tag{8}$$

where I_P and I_Q are intensities of light from points P and Q, respectively, and ϕ is the phase difference between the light rays from P and Q. The last term of Eq. (8) represent the intensity of interference of the light rays from P and Q.

If a load is applied to the specimen, the specimen would be deformed, and the displacement of points P and Q are, in general, represented by (u, v, w) and $(u + \delta u, v + \delta v, w + \delta w)$, respectively, in the x, y, and z directions. These produce a further phase shift Δ between the light paths to point O in the image plane. Equation (8) then becomes

$$I'_O = I_P + I_Q + 2\sqrt{I_P I_Q}\cos(\phi + \Delta) \tag{9}$$

During the measuring process, the intensity distribution $I(x, y)$ of a speckle pattern is recorded by the CCD camera and then stored in one frame. After the loading is changed, the intensity distribution $I'(x, y)$ of the speckle pattern is slightly altered. It is recorded and stored in another frame. A fringe pattern, called a digital shearogram, is produced when the absolute value of the difference between the two frames is calculated; this process is called digital frame subtraction. In the shearogram, a bright fringe occurs when the relative phase change Δ between the two frames is equal to $(2n + 1)\pi$, whereas a dark fringe corresponds to $\Delta = 2n\pi$,

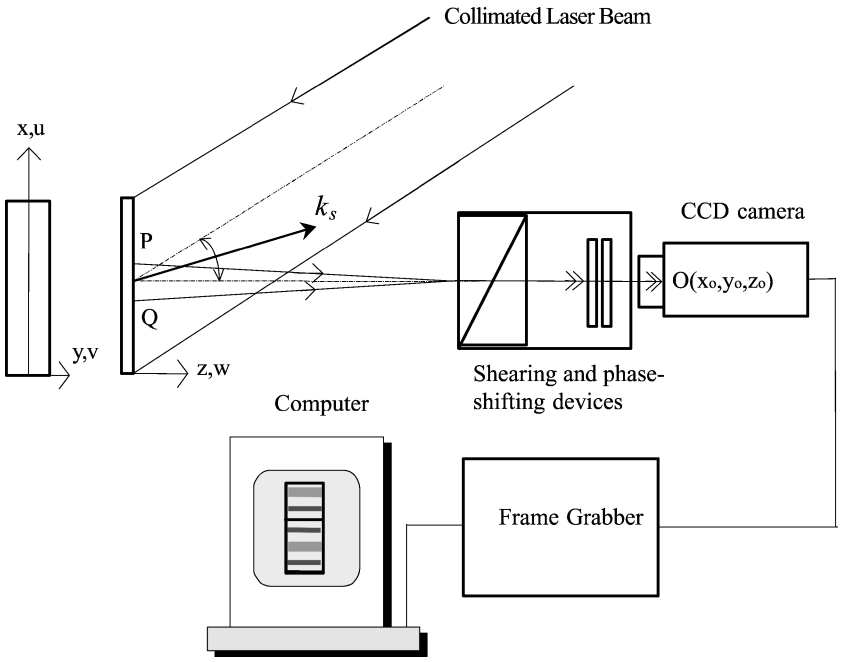

Fig. 2 Schematic diagram of the optical setup of a typical phase-shifting digital speckle shearing interferometer.

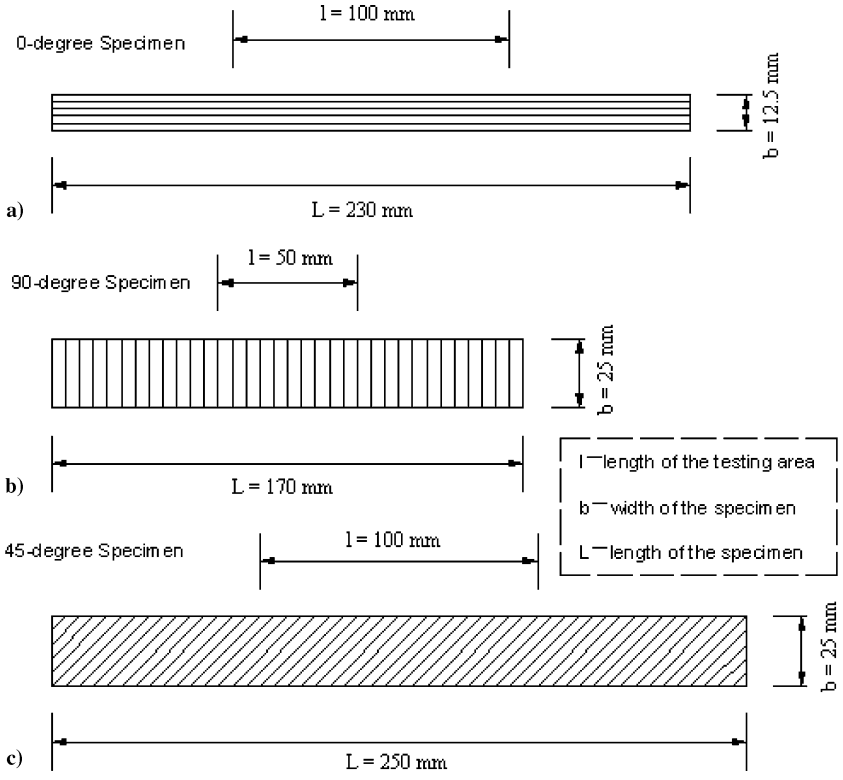

Fig. 3 Three types of tension test specimen usually used in the classical experiment according to ASTM C1341 standard.[3]

where $n = 0, \pm1, \pm2, \pm3, \ldots$, is the fringe order. Digital subtraction can be executed on a personal computer at video rate by software. The digital shearogram therefore can be observed in real time.

Owing to the nature of shearing, the phase change Δ in ESSI is related to the displacement derivatives instead of the displacement itself. If the shearing direction is in the x direction, Δ is given by

$$\Delta_x = \left(\frac{\partial u}{\partial x}\boldsymbol{k}_s \cdot \boldsymbol{e}_x + \frac{\partial v}{\partial x}\boldsymbol{k}_s \cdot \boldsymbol{e}_y + \frac{\partial w}{\partial x}\boldsymbol{k}_s \cdot \boldsymbol{e}_z\right)\delta x \qquad (10)$$

Where the shearing direction lies in the y direction, Δ is given by

$$\Delta_y = \left(\frac{\partial u}{\partial y}\boldsymbol{k}_s \cdot \boldsymbol{e}_x + \frac{\partial v}{\partial y}\boldsymbol{k}_s \cdot \boldsymbol{e}_y + \frac{\partial w}{\partial y}\boldsymbol{k}_s \cdot \boldsymbol{e}_z\right)\delta y \qquad (11)$$

where u, v, w represent the components of the displacement vector and $\boldsymbol{e}_x, \boldsymbol{e}_y, \boldsymbol{e}_z$ represent the unity vectors in the x, y, and z directions, respectively; $\boldsymbol{k}_s$ is the sensitivity vector, which lies along the bisector of the angle between the illuminating and viewing directions as shown in Fig. 2.

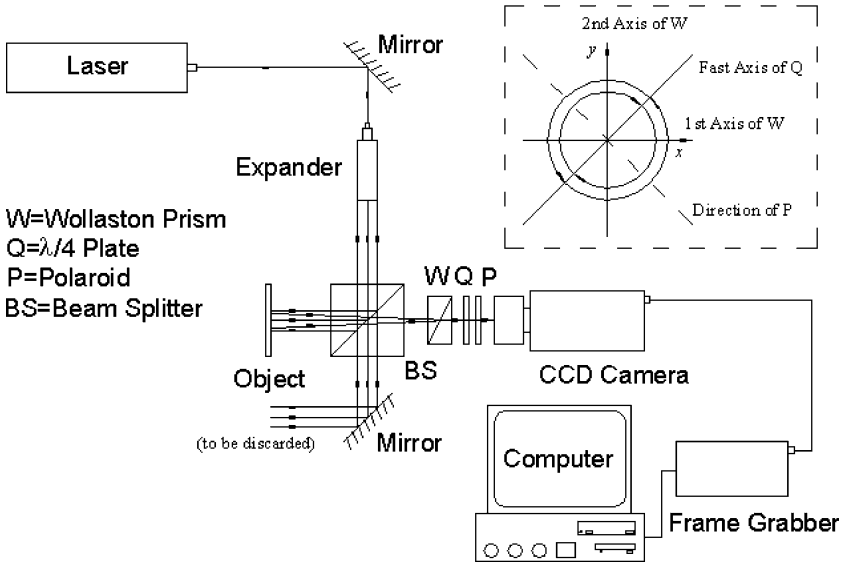

Fig. 4 Schematic diagram of the optical setup of the proposed phase-shifting digital speckle shearing interferometer.

The derivatives of out-of-plane displacement $\partial w/\partial x$ and $\partial w/\partial y$ can be directly measured by shearography if normal illumination and normal observation are adopted. In this case, the sensitivity vector $\boldsymbol{k}_s$ lies exactly in the z direction so that $\boldsymbol{k}_s \cdot \boldsymbol{e}_x = \boldsymbol{k}_s \cdot \boldsymbol{e}_y = 0$ and $\boldsymbol{k}_s \cdot \boldsymbol{e}_z = |\boldsymbol{k}_s| = 4\pi/\lambda$, where λ is the wavelength of the laser beam. Now Eqs. (10) and (11) are reduced to the following:

x-direction shearing

$$\Delta_x = \frac{\partial w}{\partial x}|\boldsymbol{k}_s|\delta x = \frac{4\pi\delta x}{\lambda}\frac{\partial w}{\partial x} \tag{12}$$

y-direction shearing

$$\Delta_y = \frac{\partial w}{\partial y}|\boldsymbol{k}_s|\delta y = \frac{4\pi\delta y}{\lambda}\frac{\partial w}{\partial y} \tag{13}$$

The in-plane strains $\partial u/\partial x$ and $\partial v/\partial y$ cannot be measured directly by adjusting the illuminating direction or the observing direction because the sensitivity vector $\boldsymbol{k}_s$ will never fall exactly in the x or y direction and measurement errors would be incurred. A solution to measuring in-plane strain is the utilization of two alternate illumination directions. Considering two illuminating beams in the xz plane angled $\pm\theta$ to the shearing direction, the x direction, we can express the shearogram from Eq. (10) as

$$\begin{aligned}\Delta_{+\theta} &= \frac{2\pi}{\lambda}\left\{\frac{\partial u}{\partial x}\sin(+\theta_{xz}) + \frac{\partial w}{\partial x}[1+\cos(+\theta_{xz})]\right\}\delta x \\ \Delta_{-\theta} &= \frac{2\pi}{\lambda}\left\{\frac{\partial u}{\partial x}\sin(-\theta_{xz}) + \frac{\partial w}{\partial x}[1+\cos(-\theta_{xz})]\right\}\delta x\end{aligned} \tag{14}$$

Because $\sin(-\theta) = -\sin\theta$ and $\cos(-\theta) = \cos\theta$, the in-plane strain $\partial u/\partial x$ can now be determined by subtracting Δ_θ from $\Delta_{+\theta}$:

$$\Delta_I = \Delta_{+\theta} - \Delta_{-\theta} = \frac{4\pi\delta x\sin\theta_{xz}}{\lambda}\frac{\partial u}{\partial x} \tag{15}$$

The relative phase change $\Delta_{-\theta}$ from $\Delta_{+\theta}$ can be calculated quantitatively at each pixel point using phase-shift technique.[14] The phase distribution Δ_I can be obtained simply from the difference between the two fringe patterns $\Delta_{-\theta}$ and $\Delta_{+\theta}$. The result is a new fringe pattern depicting the pure in-plane strain $\partial u/\partial x$. Other in-plane strain components $\partial u/\partial y$, $\partial v/\partial x$, and $\partial v/\partial y$ can be determined in a similar way when the shearing and the illuminating directions are set properly.

In view of the complication of the optical measurement of in-plane strains as just mentioned, we proposed the evaluation of the elastic properties of a composite beam by measuring the out-of-plane deformation gradient $\partial w/\partial x$ instead. Normal illumination and observation is achieved by using a beam splitter as illustrated in Fig. 4. The laser beam is reflected by a mirror and then expanded by an expander. The beam splitter turns the incident expanded beam into two. One of them is made to illuminate the object normally. The other one is discarded by a beam stop. The diffused reflection intensity of the object surface is imaged by a CCD camera through a series of optical device. The beam splitter also makes the observation direction normal to the image plane. The shearing and phase-shifting device introduces shearing as well as a phase shift to perform quantitative measurement. The shearing and phase-shifting device is made of a set of polarizers, a Wollaston prism W, a quarter-wave retarder Q, and a polaroid P. The object is illuminated by an expanded parallel laser beam and imaged by a CCD camera with the device in front of the image lens. A Wollaston prism acts as the shearing device to split an incoming beam into two separate orthogonally linearly polarized beams. The quarter-wave retarder, whose fast axis is oriented at 45 deg to the two material axes of the Wollaston prism, turns the two beams into two circularly polarized beams with different rotational directions. The polaroid makes the two related beams interfere. In the image plane, an interferogram called a speckle pattern is produced. Moreover, phase shift can be easily introduced by rotating the polaroid.[17]

The phase Δ can be evaluated quantitatively by phase-shift technology. A four-step phase-shift technique[14] is employed. The four phase steps are 0, π, $\pi/2$, and $3\pi/2$, and they are introduced into the interferometer by rotating the polaroid to the corresponding angles. Four images of the specimen with different phase shifts are acquired before the specimen is loaded. They can be expressed as

$$\begin{aligned}I1 &= I_P + I_Q + 2\sqrt{I_P I_Q}\cos\phi \\ I2 &= I_P + I_Q + 2\sqrt{I_P I_Q}\cos(\phi+\pi/2) \\ &= I_P + I_Q - 2\sqrt{I_P I_Q}\sin\phi \\ I3 &= I_P + I_Q + 2\sqrt{I_P I_Q}\cos(\phi+\pi) \\ &= I_P + I_Q - 2\sqrt{I_P I_Q}\cos\phi \\ I4 &= I_P + I_Q + 2\sqrt{I_P I_Q}\cos(\phi+3\pi/2) \\ &= I_P + I_Q + 2\sqrt{I_P I_Q}\sin\phi\end{aligned} \tag{16}$$

After the loading is applied to the specimen, another group of four images is acquired. They can be expressed as

$$
\begin{aligned}
I5 &= I_P + I_Q + 2\sqrt{I_P I_Q}\cos(\phi + \Delta) \\
I6 &= I_P + I_Q + 2\sqrt{I_P I_Q}\cos(\phi + \Delta + \pi/2) \\
&= I_P + I_Q - 2\sqrt{I_P I_Q}\sin(\phi + \Delta) \\
I7 &= I_P + I_Q + 2\sqrt{I_P I_Q}\cos(\phi + \Delta + \pi) \\
&= I_P + I_Q - 2\sqrt{I_P I_Q}\cos(\phi + \Delta) \\
I8 &= I_P + I_Q + 2\sqrt{I_P I_Q}\cos(\phi + \Delta + 3\pi/2) \\
&= I_P + I_Q + 2\sqrt{I_P I_Q}\sin(\phi + \Delta)
\end{aligned} \tag{17}
$$

We can deduce the phases ϕ and $\phi + \Delta$ from Eqs. (16) and (17) as

$$
\tan\phi = \frac{I4 - I2}{I1 - I3}
$$

$$
\tan(\phi + \Delta) = \frac{I8 - I6}{I5 - I7} \tag{18}
$$

However, the phases ϕ and $\phi + \Delta$ obtained by calculating $\arctan[(I4 - I2)/(I1 - I3)]$ and $\arctan[(I8 - I6)/(I5 - I7)]$ are "wrapped" in the range of $[0\ 2\pi]$. They can be expressed as

$$
\phi_w = \arctan\left(\frac{I4 - I2}{I1 - I3}\right)
$$

$$
(\phi + \Delta)_w = \phi_w + \Delta_w = \arctan\left(\frac{I8 - I6}{I5 - I7}\right) \tag{19}
$$

The wrapped phase Δ_w is evaluated by

$$
\Delta_w = \arctan\left(\frac{I8 - I6}{I5 - I7}\right) - \arctan\left(\frac{I4 - I2}{I1 - I3}\right) \tag{20}
$$

An unwrapping operation[11] is required to be performed on Δ_w in order to obtain Δ.

The mechanical part of the measurement system is described in the following. A 0-deg beam specimen as shown in Fig. 3a is loaded in the four-point bending condition as illustrated in Fig. 5. The beam specimen is simply supported near the two ends and loaded at points one-quarter and three-quarter of the beam length so that the middle part of the beam is in a state of pure bending. As far as the middle part of the beam is concerned, the bending moment can be expressed as

$$
M = \frac{FL}{8} = E_1 I \frac{\partial^2 w}{\partial x^2} = E_1 \frac{bh^3}{12}\frac{\partial^2 w}{\partial x^2} \tag{21}
$$

where L, b, h are the length, width, and height of the specimen, respectively; w is the displacement along the z direction; E_1 is the Young's modulus parallel to the fibers; I is the cross-section modulus, and F is the transverse loading.

As shown in Eq. (12), ESSI can measure the wrapped phase proportional to the displacement gradient $\partial w/\partial x$. For the four-point bending, the displacement gradient is linear along the x direction in the beam span $L/4 < x < 3L/4$. From Eq. (12), we can write

$$
\frac{\partial w}{\partial x} = kx = \frac{\Delta_x \lambda}{4\pi\delta_x} \tag{22}
$$

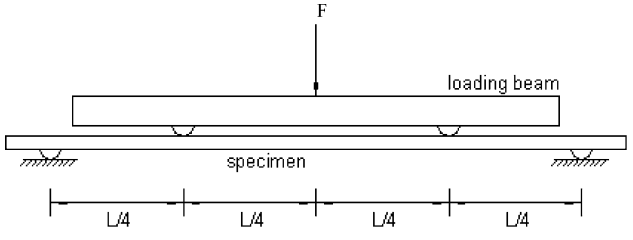

Fig. 5 Four-point bending configuration.

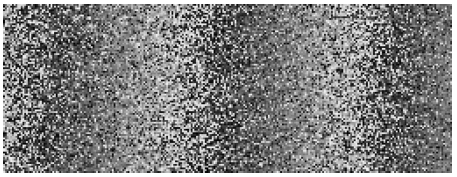

a) Phase map of a composite beam under pure bending (*S*)

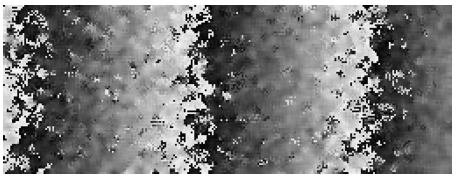

b) Enhanced phase map by double-field adaptive filter (*ES*)

c) Unwrapped phase map (*US*)

Fig. 6 Phase maps of the composite specimen.

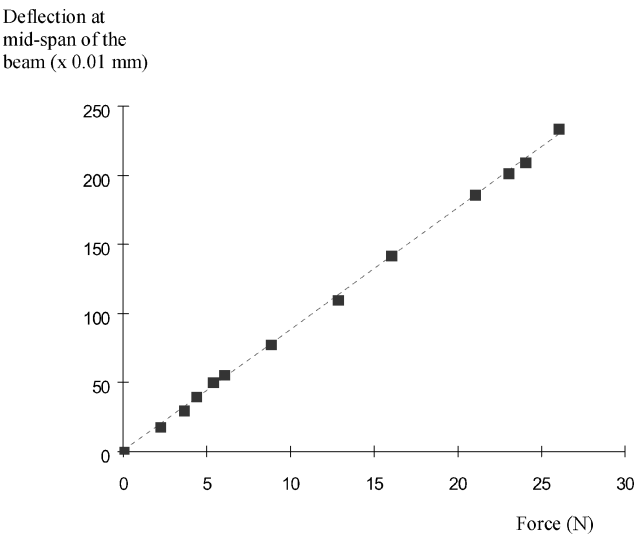

Fig. 7 Load-deflection plot of the CFRP specimen.

where k is a constant. The curvature of the beam along the x axis can be written as

$$
\frac{\partial^2 w}{\partial x^2} = k = \frac{\lambda}{4\pi\delta_x}\left(\frac{\Delta_x}{x}\right) \tag{23}
$$

If c is the slope of the graph of phase Δ_x vs the pixel number as shown in Fig. 6 and r the scaling factor of the interferogram that represent how long on the specimen surface a pixel in the image indicates, we can write

$$
\Delta_x / x = c/r \tag{24}
$$

From Eqs. (20–23), the Young's modulus E_1 can be written as

$$
E_1 = \frac{6\pi F L \delta_x r}{\lambda b h^3 c} \tag{25}
$$

The Poisson's ratio μ and shear modulus G of the orthrotropic material are evaluated based on the following principle.

Consider the moment-curvature relationship of a laminate symmetric in both geometry and material properties about the middle surface, subject to bending only:

$$\begin{Bmatrix} \dfrac{\partial^2 w}{\partial x^2} \\ \dfrac{\partial^2 w}{\partial y^2} \\ \dfrac{2\partial^2 w}{\partial x \partial y} \end{Bmatrix} = \frac{3}{h^3} \begin{bmatrix} \bar{S}_{11} & \bar{S}_{12} & \bar{S}_{16} \\ \bar{S}_{12} & \bar{S}_{22} & \bar{S}_{26} \\ \bar{S}_{16} & \bar{S}_{26} & \bar{S}_{66} \end{bmatrix} \begin{Bmatrix} M_x \\ M_y \\ M_{xy} \end{Bmatrix} \tag{26}$$

or in the matrix form

$$\{K\} = (3/h^3)[\bar{S}]\{M\} \tag{27}$$

where $\{K\}$ is the curvature vector of the unidirectional lamina and $[\bar{S}]$ is the generalized compliance matrix shown in Eq. (7). When only M_x acts on the strip, Eq. (26) becomes

$$\frac{\partial^2 w}{\partial x^2} = \frac{3\bar{S}_{11} M_x}{h^3}$$

$$\frac{\partial^2 w}{\partial y^2} = \frac{3\bar{S}_{12} M_x}{h^3}$$

$$\frac{\partial^2 w}{\partial x \partial y} = \frac{1.5\bar{S}_{16} M_x}{h^3} \tag{28}$$

If the x axis is parallel to the fiber axis,

$$\bar{S}_{11} = S_{11} = \frac{1}{E_1} = \left(\frac{h^3}{3M_x}\right)\left(\frac{\partial^2 w}{\partial x^2}\right) \tag{29}$$

E_1 then can be measured from the bending test of a 0-deg specimen. If the x axis is perpendicular to the fiber axis,

$$\bar{S}_{11} = S_{22} = \frac{1}{E_2} = \left(\frac{h^3}{3M_x}\right)\left(\frac{\partial^2 w}{\partial x^2}\right) \tag{30}$$

E_2 can therefore be measured from the bending test on a 90-deg specimen. If the x axis is at 45 deg to the fiber axis,

$$\bar{S}_{11} = \frac{1}{4}\left(\frac{1}{E_1} + \frac{1}{E_2} - 2\frac{\mu_{12}}{E_1} + \frac{1}{G}\right) = \left(\frac{h^3}{3M_x}\right)\left(\frac{\partial^2 w}{\partial x^2}\right)$$

$$\bar{S}_{12} = \frac{1}{4}\left(\frac{1}{E_1} + \frac{1}{E_2} - 2\frac{\mu_{12}}{E_1} - \frac{1}{G}\right) = \left(\frac{h^3}{3M_x}\right)\left(\frac{\partial^2 w}{\partial y^2}\right) \tag{31}$$

In the bending test on a 45-deg specimen, curvatures $\partial^2 w/\partial x^2$ and $\partial^2 w/\partial y^2$ are measured. Afterwards, the Poisson's ratio μ_{12} and shear modulus G can be deduced from Eq. (31). The Poisson's ratio μ_{21} can be obtained from the formula

$$\mu_{12}/E_1 = \mu_{21}/E_2 \tag{32}$$

IV. Experimental Results

A. Specimens

Nine specimens of sizes and orientations of those as shown in Figs. 3a–3c were cut using a milling machine from a large piece of unidirectional glass fiber-reinforced composite panel brought from the Nanjing Xingya FRP Co., Ltd., of the People's Republic of China. The specimen has three laminas. The fibers in the top and the bottom laminas each of about 10% thickness of the specimen had a random orientation while the orientation of the fibers in the middle laminate was unidirectional. As just noted, fiber orientation of 0, 45, and 90 deg to the beam axis were tested. The fiber volume ratio of the specimen was 40%.

Table 1 Measured Young's modulus of a steel specimen and a composite specimen

Material property	Steel specimen, 249.3 × 12.59 ×5.80 mm	Composite specimen E_1, 230.8 mm × 12.26 mm ×5.08 mm
Mass, g	140.18	26.25
Young's modulus by vibration test (ASTM C1259), GPa	198.4	24.98
Young's modulus by tensile test (ASTM C1341), GPa	197.8	24.91
Young's modulus by the proposed optical test, GPa	195.6	24.95
Difference between the tensile test result and the optical test result, %	1.1	0.16

A steel specimen of similar dimensions to the 0-deg composite specimen was also made and tested before the composite specimens by the three methods as described in the following. The dimensions of the steel and composite specimens are shown in Table 1. The nine glass fiber reinforced plastic specimens were divided into three groups each of three specimens. Each group of the specimens was tested by one of the following three methods.

B. Standard Tensile Test

It is necessary to prove the optical measurement to be reliable by comparing its results with those obtained by other standard methods. Mechanical measurements based on strain gauges are considered first.

The traditional mechanical measurement adopts the stress–strain relations in Eqs. (5) and (6). There are three test steps. First, consider uniaxial tension loading in the one-direction on a 0-deg specimen shown in Fig. 3a. The strains ε_1 and ε_2 are measured, and by definition

$$\sigma_1 = P/A, \qquad E_1 = \sigma_1/\varepsilon_1, \qquad \mu_{21} = -(\varepsilon_2/\varepsilon_1) \tag{33}$$

where A is cross-sectional area of the test section perpendicular to the applied load. Second, consider uniaxial tension loading in the two direction on a 90-deg specimen shown in Fig. 3b. Similar to the first measurement, ε_1 and ε_2 are measured so

$$\sigma_2 = P/A, \qquad E_2 = \sigma_2/\varepsilon_2, \qquad \mu_{12} = -(\varepsilon_1/\varepsilon_2) \tag{34}$$

The stiffness properties satisfy the reciprocal relations in Eq. (32). Third, consider uniaxial tension loading at 45 deg to the one direction on the 45-deg specimen shown in Fig. 3c. The remaining properties G_{12} is then determined. By measurement of ε_x alone, obviously

$$E_x = (P/A)/\varepsilon_x \tag{35}$$

By use of this modulus transformation relations in Eq. (7) supposing $\theta = 45$ deg, we get

$$G_{12} = 1/(4/E_x - 1/E_1 - 1/E_2 + 2\mu_{12}/E_1) \tag{36}$$

Accordingly, the shear modulus G_{12} can be found.

Before the experiment, strain gauges were strongly attached to the surface of the specimens. They were laid in the directions prescribed in the preceding text. Their leads were attached to the specimen and linked to a strain meter. During the experiment, the specimens were put into tension by the loading machine (MTS Alliance RT/50). The values of the loading and the corresponding readings of the strains meter were recorded. Measurement data were then processed to evaluate the elastic properties of the composite material. The result is presented in Table 2.

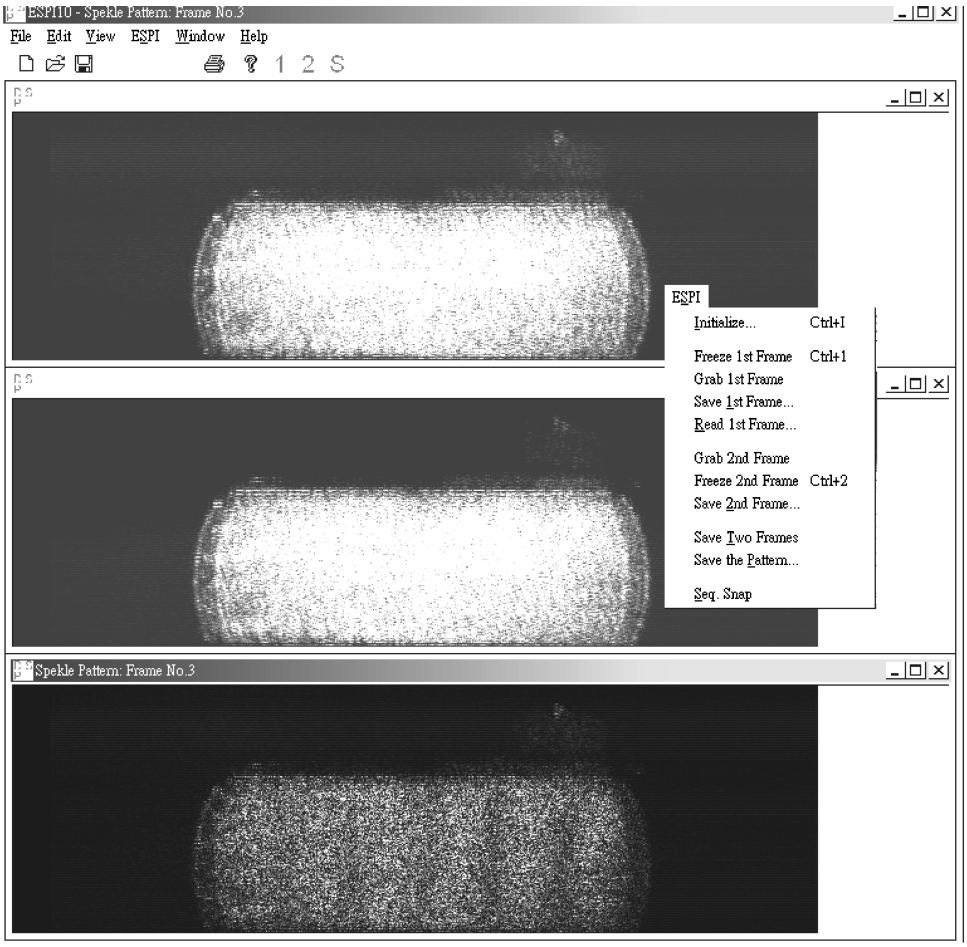

Fig. 8 Computer interface of the self-developed digital speckle shearing interferometry software.

Table 2 Elastic properties of the composite specimen measured by a standard tensile test and the proposed optical method

Composite	Tensile test (ASTM C1341)	Optical (the proposed method)	Percentage difference
E_1	24.92 GPa	24.95 GPa	0.1
E_2	4.21 GPa	4.26 GPa	1
G_{12}	2.07 GPa	1.97 GPa	5
μ_{12}	0.36	0.31	14
μ_{21}	0.072	0.052	28

C. Standard Test by Vibration Frequencies Measurement

There is a standard test method for measuring dynamic Young's modulus, shear modulus, and Poisson's ratio introduced by the American Society for Testing and Materials (ASTM).[3] The standard, issued under the fixed designation C1259-96, measures the fundamental resonant frequency of test specimens of suitable geometry by exciting them mechanically by a singular elastic impact with an impulse tool.

According to the requirement of the standard, the free-free beam is suspended by two wires attached at the nodal points of the measured vibration mode. If the length/thickness ratio L/h of the beam is more than 20, the Young's modulus E can be calculated directly by[3]

$$E = 0.9465[1 + 6.585(h/L)^2]\left(mf_f^2/b\right)(L^3/h^3) \qquad (37)$$

where m is the mass of the beam and f_f is its fundamental resonant frequency.

The fundamental resonant frequencies of the steel and GFRP specimens were measured by a Polytec laser vibrometer and a B&K 2032 FFT spectrum analyzer and the results processed. The Young's moduli of the steel and 0-deg composite specimens were found to be 198.4 and 24.98 GPa, respectively.

D. Experimental Test by the Proposed ESSI Method

The steel and composite specimens were tested by the proposed ESSI method of principle described in Sec. III. The optical setup is shown in Fig. 4 with the following setup parameters: resolution ratio r, 0.0806 mm/pixel; shear distance Δx, 1.527 mm; and wavelength λ, 0.6328 μm.

The object shown in Fig. 4 is the bent beam loaded in four-point bending as shown in Fig. 5. Setup parameters of the four-point bending are as follows: support span length (L in Fig. 5), 200 mm; load span length, 100 mm; span-to-depth ratio, 49; and diameters of loading and support pins, 8 mm.

Dimensions of the beam specimens are shown in Table 1. Loading was applied to the beams through the four-point bending mechanism using dead weights. A load-deflection curve for the GFRP specimen was measured and is plotted in Fig. 7 to define for the linear region used for modulus determination. For the optical measurements, a He–Ne laser of 35 mW was used to generate the speckle shearing interferograms. An ESSI program was developed in house using Visual C++, and it was used for image acquisition and real-time image processing. A photograph of the computer interface with the program is shown in Fig. 8. The polaroid was set to its 0-deg orientation first, and image I_1 was acquired with a CCD camera with a frame grabber (IC4-PCI of Imaging Tech, Inc.). The polaroid was rotated to 45, 90, and 135 deg, respectively to generate images I_2, I_3, I_4. A static force was then applied slowly to the specimen by using a dead weight through the four-point bending mechanism, and the applied force F was measured as 3.5 N by using a force gauge. The real-time fringe pattern of the displacement gradients of the specimen

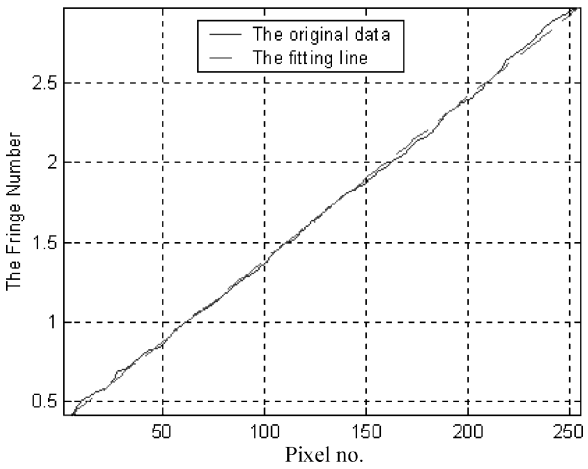

Fig. 9 Averaged unwrapped phase value vs pixel number.

was displayed on the computer monitor. Distortion or misalignment of the specimen could be observed from the fringe pattern, and they were rectified until the fringe pattern became regular. The phase-shift procedure was repeated, and images I_5, I_6, I_7, I_8 were stored. From those eight images, the phase map was calculated according to Eq. (20) and is shown in Fig. 6a. It is very noisy because of the presence of many high-frequency speckles. To elicit the slope variation ratio, low-pass filtering was performed on the phases. However, the work is not simple because of the 2π step jumping in the phase map. This problem was solved by the double-field adaptive filtering technique. The filtering can be expressed as

$$ES = \arctan \frac{f[\sin(S)]}{f[\cos(S)]} \tag{38}$$

where S is the original phase map; ES is the enhanced phase map; $f()$ is the Wienier adaptive filtering function. In Eq. (31), the sine and cosine value of the original phase was filtered by the adaptive noise-removal filter respectively, and then the phase was calculated by the filtered data. The enhanced phase map is shown in Fig. 6b.

The third step is to unwrap the phase map. The unwrapping work eliminates the 2π phase jumping and suppresses the noise as well. Generally, the phase map improved by the two filters was smooth enough to start unwrapping. The unwrapped phase map is shown in Fig. 6c. The phase map was stored in the computer as a matrix. The mean phase value of each column of the matrix was calculated, and the result is a row vector storing all of the mean values of each column of the phase matrix. The advantage of doing this is to average out the random variation of the unwrapped phase caused by the speckle noise. The unwrapped phase values are fitted by a straight line and the slope of the fitted line determined to give the constant k in Eq. (23). These are shown in Fig. 9. By Eq. (25), the Young's modulus E_1 of the steel beam can be calculated as 195.6 GPa.

The Young's modulus E_1 of the 0-deg GFRP beam was determined to be 24.95 GPa. E_2 was then measured from the 90-deg specimen and $\bar{S}_{11}$ for a 45-deg specimen, whereafter the shear direction should change from the x axis to the y direction to evaluate $\bar{S}_{12}$ for a 45-deg specimen. Using these data, all of the elastic constants were calculated. Measurement results of the nine composite specimens as shown in Tables 1 and 2 are mean values. Variability of the measured moduli in all three of the methods is less than 5%.

E. Discussion of the Experimental Results

A comparison of the measurements of the elastic constants for the steel and the 0-deg GFRP specimens by the three different methods is shown in Table 1. It is clear that, comparing these results, for the steel (isotropic material) and the unidirectionally fiber-reinforced composite (orthotropic material), the proposed optical technique can provide results similar to those from the standard tests. The elastic moduli and Poisson's ratio of the composite laminate measured by the standard tensile test and the proposed optical test are shown in Table 2. The moduli results of the two methods are similar, whereas the differences in the Poisson's ratios are quite large. The accuracy of the moduli E_1 and E_2 depends on the accuracy of the values of displacement gradients and also on the accuracy of the thickness measurement. The accuracy in the measurement of the displacement gradients using the ESSI method is estimated to be within $\pm 0.5\%$ of the maximum displacement gradient measured. The thickness measurement has an accuracy of ± 0.01 mm.

The error of μ_{12} can be caused by the fact that it is calculated from Eq. (31), and its error is sensitive to the measurement errors of $\partial^2 w/\partial x^2$ and $\partial^2 w/\partial y^2$. The large error in μ_{21} is the accumulation of the errors in μ_{12}, E_1 and E_2 because it is calculated from Eq. (32). This error can be reduced if μ_{21} is measured by a procedure similar to μ_{12} (with the x axis at 135 deg to the fiber axis). These errors seem to be reasonable as they are similar to those reported by other researchers.[18] Analysis of some major error sources can be found in Ref. 18.

V. Conclusions

A new optical method for the measurement of elastic material properties using speckle interferometry is proposed. A speckle shearing interferometer with simple setup is devised for the direct full-field characterization of the elastic properties of isotropic materials and orthotropic laminates. The technique developed in this project has the potential to provide a valuable nondestructive noncontact tool for material characterization for use in industry and can even be carried out in a workshop environment. This is feasible because most of the light paths in the shearing interferometry setup are common and the process has the advantage of being relatively vibration insensitive. Both the theoretical studies of the method of measurement and the experimental results are presented.

Acknowledgments

The work described in this paper was substantially supported by a grant from the Hong Kong Polytechnic University (A-P201) and another grant from the Research Grants Council of the Hong Kong Special Administrative Region (PolyU 5172/01E) of the People's Republic of China.

References

[1]Carlsoon, L. A., and Pipes, R. B., *Experimental Characterization of Advanced Composite Materials*, Prentice–Hall, Upper Saddle River, NJ, 1987, pp. 117–124.

[2]ASTM Standard C1341, "Test Method for Flexural Properties of Continuous Fiber-Reinforced Advanced Ceramic Composites," *Annual Book of ASTM Standards*, Vol. 15.01, American Society for Testing and Materials, Philadelphia, 2002, pp. 524–542.

[3]ASTM Standard C1259, "Test Method for Dynamic Young's Modulus, Shear Modulus, and Poisson's Ratio for Advanced Ceramics by Impulse Excitation of Vibration," *Annual Book of ASTM Standards*, Vol. 15.01, American Society for Testing and Materials, Philadelphia, 2002, pp. 301–318.

[4]Pindera, M. J., and Herakovich, C. T., "Shear Characterization of Unidirectional Composite with the Off-Axis Tension Test," *Experimental Mechanics*, Vol. 26, March 1986, pp. 103–112.

[5]Pierron, F., "Saint-Venant Effects in the Iosipescu Specimen," *Journal of Composite Material*, Vol. 32, No. 22, 1998, pp. 1986–2015.

[6]Grèdiac, M., "On the Direct Determination of Invariant Parameters Governing the Bending of Anisotropic Plates," *International Journal Solids and Structure*, Vol. 33, No. 27, 1996, pp. 3969–3982.

[7]Grèdiac, M., Pierron, F., and Surrel, Y., "Novel Procedure for Complete In-Plane Composite Characterization Using a Single T-Shaped Specimen," *Experimental Mechanics*, Vol. 39, 1999, pp. 142–149.

[8]Grèdiac, M., Fournier, N., Paris, P.-A., and Surrel, Y., "Direct Identification of Elastic Constants of Anisotropic Plates by Modal Analysis: Experimental Results," *Journal of Sound and Vibration*, Vol. 210, No. 5, 1998, pp. 643–659.

[9]Ma, C. C., and Lin, C. C., "Inverse Evaluation of Material Constants for Composite Plates by Optical Interferometry Method," *AIAA Journal*, Vol. 37, No. 8, 1999, pp. 947–953.

[10]Furgiuele, F. M., Muzzupappa, M., and Pagnotta, L., "A Full-Field Procedure for Evaluating the Elastic Properties of Advanced Ceramics," *Experimental Mechanics*, Vol. 37, No. 3, 1997, pp. 285–291.
[11]Surrel, Y., "Design of Algorithms for Phase Measurements by the Use of Phase-Stepping," *Applied Optics*, Vol. 35, No. 1, 1997, pp. 51–60.
[12]Wong, W. O., Chan, K. T., and Leung, T. P., "Identification of Anti-Nodes and Zero-Surface-Strain Contours of Flexural Vibration with Time-Average Speckle Pattern Shearing Interferometry," *Applied Optics*, Vol. 106, No. 16, 1997, pp. 3776–3784.
[13]Wong, W. O., "A Simple Speckle Shearing Interferometer," *Optics and Laser Technology*, Vol. 34, No. 5, 2002, pp. 399–403.
[14]Creath, K., "Phase-Shifting Holographic Interferometry," *Holographic Interferometry, Principles and Methods*, edited by P. K. Rastogi, Springer-Verlag, Berlin, 1994, pp.109–150.
[15]Jones, R. M., *Mechanics of Composite Materials*, Taylor and Francis, Philadelphia, 1999, pp. 31–47.
[16]Jones, R., and Wykes, C., *Holographic and Speckle Interferometry*, 2nd ed. Cambridge Univ. Press, Cambridge, England, U.K., 1989, pp. 156–159.
[17]Jin, G. C., Bao, N. K., and Chung, P. S., "A New Computer-Controlled Polarization Phase-Shifting Technique," *Proceedings of the International Society for Optical Engineering*, Vol. 2066, *Industrial Optical Sensing and Metrology: Applications and Integration*, edited by K. G. Harding, Society of Photo-Optical Instrumentation Engineers, Bellingham, WA, 1993, pp. 67–71.
[18]Bruno, L., Furgiuele, F. M., Pagnotta, L., and Poggialini, A., "A Full-Field Approach for the Elastic Characterization of Anisotropic Materials," *Optics and Lasers in Engineering*, Vol. 37, No. 4, 2002, pp. 417–431.

K. Shivakumar
Associate Editor